Spontaneous emission mechanisms of GaInAsN/GaAs quantum dot systems

Z. F. Wei, S. J. Xu,[a] and Q. Li
Department of Physics and HKU-CAS Joint Laboratory on New Materials, The University of Hong Kong, Pokfulam Road, Hong Kong, China

(Received 28 April 2006; accepted 6 October 2006; published online 22 December 2006)

Variable-temperature photoluminescence (PL) spectra taken on two different kinds of GaInAsN quantum dots (QDs), having different In and N compositions and thicknesses, have been investigated both experimentally and theoretically. It is found that the temperature dependence of the spontaneous emissions from both samples behaves differently. Adopting a localized-state luminescence model, the quantitative reproduction of the measured variable-temperature PL spectra reveals a dissimilarity in luminescence mechanisms of the two samples. These results enrich the present understanding of the luminescence mechanisms in the GaInAsN QD systems and are important for design and improvement of GaInAsN QDs based light-emitting devices. © *2006 American Institute of Physics*. [DOI: 10.1063/1.2401051]

I. INTRODUCTION

Long-wavelength semiconductor lasers emitting at 1.3–1.5 μm are key devices in the modern optical fiber communication networks. Conventionally, these lasers are made of compounds grown on InP substrates. However, the high cost and fragility of InP-based devices forced search for alternatives. Among these are dilute nitrides such as GaInAsN grown on GaAs substrates. Since this new class of materials was proposed by Kondow *et al.*,[1] they have attracted a significant research effort from both academy and industry. Although lasing actions of GaInAsN low-dimensional structures have been demonstrated, some challenging issues such as low luminescence efficiency still remain.[2] Presently, quantum wells (QWs) and quantum dots (QDs) of GaInAsN are being widely studied.[3–15] Compared to the QW systems, QD systems are expected to have higher luminescence efficiency and a lower threshold current for lasing action. The growth and characterization of $Ga_{1-y}In_yAs_{1-x}N_x$ QDs and, in particular, self-assembled QDs on GaAs substrates are thus attracting an increasing interest. In fact, Tu *et al.*[6] had already observed structural and optical evidences for the existence of QD-like nanostructures due to the phase separation effect in GaInAsN/GaAs QW structures before they intentionally grew self-assembled GaInAsN QDs.[9] Like the case of QWs, the luminescence mechanism of GaInAsN QDs is not clear at present. Very recently, we have investigated the variable-temperature photoluminescence (PL) spectra of a thick GaInAsN QD layer.[16] The obtained preliminary results indicate that the recombination mechanism of the thick GaInAsN QD layer could be very different from that of the conventional thin GaInAs QD layer.[17] The difference in electronic structure between the thick GaInAsN and thin GaInAs QDs is suggested to be responsible for the different behaviors in the spontaneous emission between them. In order to get a better understanding of the luminescence mechanisms of GaInAsN QDs, we report here a detailed comparative study on the two kinds of GaInAsN QD samples with very different thicknesses. Again, very different luminescence behaviors are found for the thin and thick GaInAsN QD samples. Quantitative simulations of the variable-temperature PL spectra of the samples using a localized-state luminescence model enable us to uncover the physical origins that cause the different luminescence behaviors of the samples.

II. EXPERIMENT

Both samples were grown on (001) GaAs substrates in a solid-source molecular beam epitaxy system equipped with a radio-frequency (rf) nitrogen plasma source. rf power was used to control the N composition in the quaternary material system. Following a 100 nm thick GaAs buffer layer grown at 580 °C, the GaInAsN QD layers were grown at 480 °C. For sample A, the growth thickness of the $Ga_{0.5}In_{0.5}As_{0.994}N_{0.006}$ QD layer was 7.6 monolayer (ML) (monolayer), whereas for sample B, the growth thickness of $Ga_{0.7}In_{0.3}As_{0.995}N_{0.005}$ QD layer was as large as 45 ML. Finally, the structures were capped by a thin layer of GaAs. The growth thickness of the quaternary QD layer was controlled by adjusting the growth rate and duration time. The nominal N composition was determined by fitting the x-ray diffraction (XRD) data from GaAsN QWs using the dynamical theory. The growth process was *in situ* monitored by reflection high energy electron diffraction (RHEED). The detailed growth description may be found in a previous publication.[13]

The variable-temperature PL measurements were taken for both samples in the temperature range from 10 to 300 K. The samples were mounted on the cold finger of a Janis closed cycle cryostat. In the variable-temperature PL measurements, the 488 nm line of an argon-krypton mixed gas laser was used as the excitation light. The luminescence signal was dispersed by an Acton SP300 monochromator and detected by a liquid-nitrogen-cooled Hamamatsu R5509 photomultiplier tube (PMT) detector. The detection wavelength

[a]Author to whom correspondence should be addressed; electronic mail: sjxu@hkucc.hku.hk

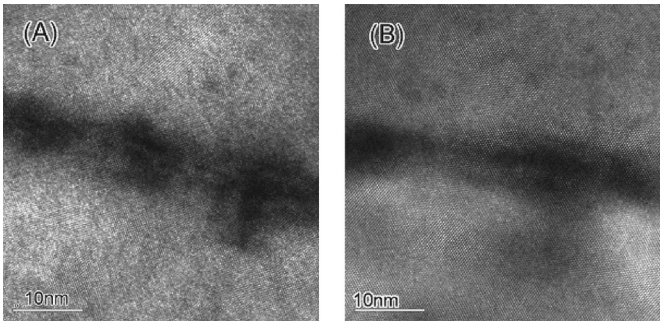

FIG. 1. Cross-sectional TEM images of the two GaInAsN QD samples: (a) $Ga_{0.5}In_{0.5}As_{0.994}N_{0.006}$ QDs and (b) $Ga_{0.7}In_{0.3}As_{0.995}N_{0.005}$ QDs.

range was from 300 to 1700 nm. In order to get the structural information on the samples, cross-sectional transmission electron microscopy (TEM) measurements were made using a JEOL 2010F microscope with a lattice resolution of 0.102 nm at Scherzer defocus. For these measurements standard TEM specimen preparation was performed.

III. RESULTS AND DISCUSSION

Figure 1 shows the cross-sectional TEM images for both samples. As expected, the GaInAsN islandlike nanostructures can be clearly observed as the dark regions due to phase contrast induced by the residual lattice-mismatch strain. For sample A, as mentioned earlier, the growth thickness of the $Ga_{0.5}In_{0.5}As_{0.994}N_{0.006}$ QD layer is only 7.6 ML due to higher In and N concentrations causing a larger mismatch strain between the dot layer and GaAs underlying layer. The lateral size of islands is seen to be around 10 nm, while their heights vary from 4 to 12 nm. As will be seen later, the severe nonuniformity in height results in significant broadening of the PL band. For sample B, due to its lower N concentration and, in particular, its lower In concentration, there is a smaller lattice-mismatch strain, and the growth thickness of the $Ga_{0.7}In_{0.3}As_{0.995}N_{0.005}$ dot layer grows to 45 ML before the RHEED spotty patterns, indicating that formation of the islands appear. In sharp contrast to the case of the 7.6 ML $Ga_{0.5}In_{0.5}As_{0.994}N_{0.006}$ QDs, the $Ga_{0.7}In_{0.3}As_{0.995}N_{0.005}$ dots are likely much more uniform. This is evidenced by the narrow PL band shown later. Energy dispersive x-ray (EDX) analysis of elemental compositions for both samples was also performed, as shown in Fig. 2. The microanalysis regions are marked by A, B, and C in the upper high-resolution TEM images of samples A and B. For both samples, region B is located within their dot layers. The EDX signals of Ga, As, and In in A, B, and C regions of the two samples are shown in the bottom figure. It is clear that the In composition of the dots in sample A is higher than that of the dots in sample B. However, the EDX signal from the N atoms could not be detected due to its extremely low composition in both samples.

Figure 3 shows the semilogarithmic variable-temperature PL spectra of the two samples. Note that the PL spectra at different temperatures have been shifted in the vertical direction to help comparison. At 10 K, the PL band of sample A peaks at 1.13 eV and has a large 54.5 meV linewidth. The broad emission band, which is related to the

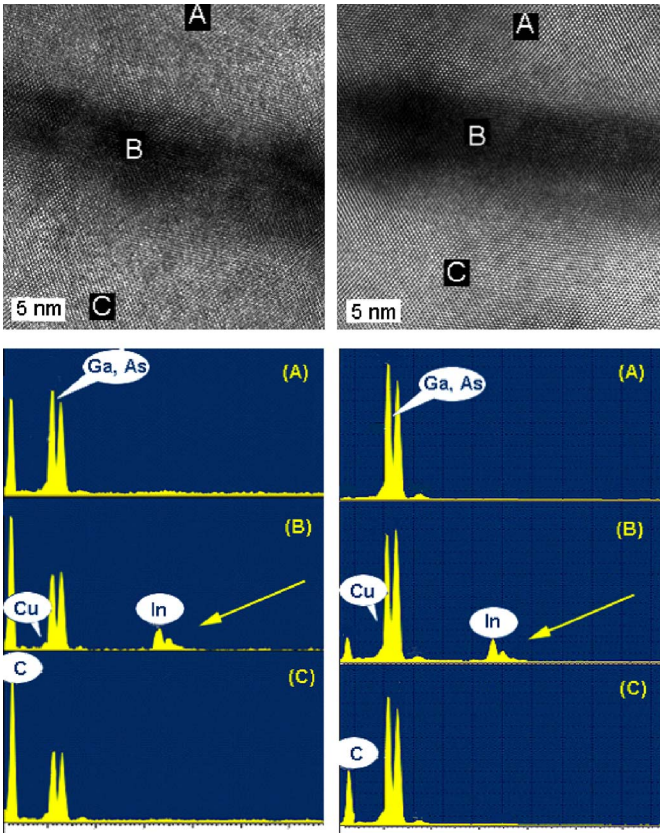

FIG. 2. (Color online) EDX analysis of elemental compositions in different regions in samples A and B. (Upper) The microanalysis regions marked by A, B, and C in the high-resolution TEM images of both samples. (Bottom) EDX signals of various elemental compositions in the regions A, B, and C of both samples. Titled arrows indicate the EDX signal of In atoms.

large nonuniformity of dots in sample A, is consistent with the TEM observation discussed earlier. Sample B, on the other hand, with its relatively narrow size distribution of dots, has its PL band centers at 1.16 eV and a full width at half maximum (FWHM) of only 13.6 meV. From Fig. 3, it can be seen that for both samples, at 10 K, their PL bands have asymmetric line shapes with a long lower energy tail. In particular, the PL band of sample B exhibits not only a long lower energy tail but also a sharp higher energy edge. The

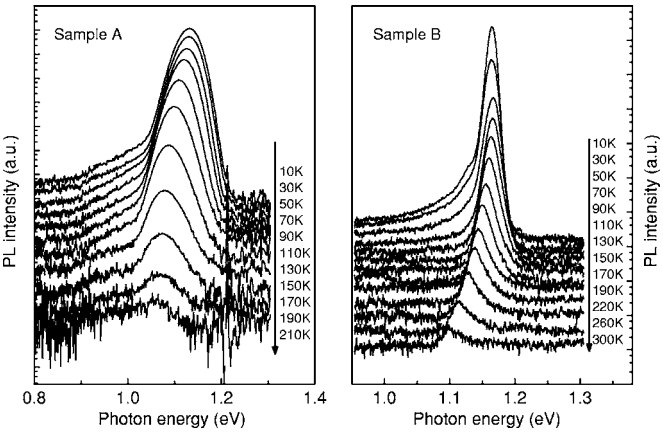

FIG. 3. Measured variable-temperature PL spectra of samples A and B. The PL spectra at different temperatures were adequately shifted for the sake of clarity.

emission tail on the lower energy side can be attributed to localized states with lower confinement energies.[6,18] Due to the nonuniform size distribution, the dots with larger size would have ground quantum states with lower energies, leading to longer wavelength emissions. On the other hand, after the incorporation of a N content the high strain energy provides a tendency for phase separation which results in a fluctuation of the N composition. With smaller atomic radius, N atoms prefer to exist in In-rich regions in order to release the local strain energy.[6,19] Hence a lower local potential well is expected to form in the dot regions with higher In and N contents. This effect may also contribute to the lower energy tail in the luminescence band. In the present work, we are mainly concern with the temperature behaviors of the luminescence bands of the two GaInAsN QD samples. For sample B with lower In and N concentrations, the lower energy emission tail diminishes quickly with increasing temperature and becomes unobservable when the temperature is above 50 K. In contrast to the case of sample B, the lower energy emission tail of sample A always remains in the temperature range of 10–210 K. Moreover, at higher temperatures, a high energy emission tail appears in the PL band of sample B. These results indicate the existence of a significant difference in the luminescence mechanism between the two samples.

In order to make a further investigation of the spontaneous emission mechanisms for the two kinds of GaInAsN QDs, the three key spectral parameters, namely, peak position (solid squares), linewidth (solid diamonds), and integrated intensity (solid circles), are extracted from the experimental spectra and are plotted as functions of temperature in Figs. 4 and 5 for samples A and B, respectively. Note that the integrated intensities of the PL bands of the two samples have been normalized for clarity. It may be seen that sample A exhibits a typical temperature-dependent luminescence behavior, as reported previously in conventional InGaAs QD systems.[17,20] For instance, below 60 K, the luminescence band is not sensitive to the temperature variation, which is a typical characteristic due to the quantum confinement effect of QDs. When the temperature is further increased, the emission peak experiences a fast redshift and the intensity begins to rapidly drop. At the same time, the peak linewidth shows a very slight reduction ranging from 50 to 80 K. As shown in the previous works,[17,20] this behavior is caused by the thermally induced redistribution of localized carriers. At higher temperatures, the scattering from lattice phonons is greatly enhanced, resulting in a significant increase of the emission band linewidth. On the other hand, the thermal escape rate of carriers from the QDs to thermally activated nonradiative recombination centers will rapidly increase and eventually lead to the quenching of the luminescence band at 220 K.

In contrast, the luminescence band of sample B exhibits a quite different temperature dependence. For the peak position of the emission band, the redshift takes place first as the temperature is increased below 40 K, followed by a weak but clear blueshift up until 70 K. The PL peak then redshifts with further increasing temperature. A more interesting observation is in the linewidth of the luminescence band. At

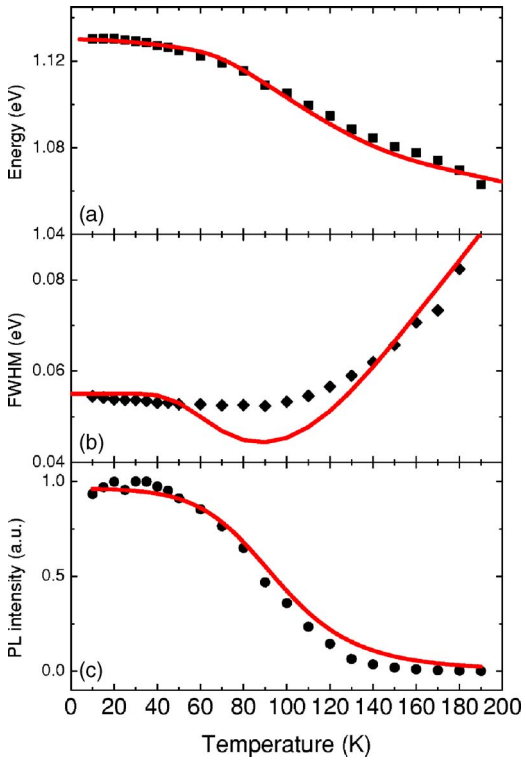

FIG. 4. (Color online) Temperature dependence of the PL spectral parameters of sample A: (a) energetic position, (b) FWHM, and (c) integrated intensity. The solid symbols are the experimental data, while the solid lines represent the calculated results using the localized-state luminescence model.

low temperatures below 40 K, the linewidth rapidly increases with temperature. Strikingly, it then keeps almost unchanged, so that a plateau appears in the linewidth-temperature curve over the temperature range of 40 to 75 K. Above 75 K the linewidth increases again. Moreover, the temperature dependence of the emission intensity of sample B is different from that of sample A. The emission intensity of sample B rapidly drops with increasing temperature below 40 K, and its quenching slows down. The above mentioned differences in the variable-temperature PL between the two samples strongly indicate that a significant difference in the underlying physical mechanism should exist for the two samples. To uncover the different physical mechanisms of the PL from both samples, a rigorous theoretical modeling is desirable.

Fortunately, we have recently developed a general model to describe the steady state luminescence from an ensemble of localized states based on a newly derived distribution function.[17] The model has been employed to quantitatively interpret the temperature behaviors of luminescence from localized carriers in very different material systems.[17,20–23] In the present work, we attempt to use this model to obtain a quantitative understanding of the observed abnormal temperature-dependent PL from the GaInAsN quantum dot samples. It is very helpful to recall the definitions and physical meanings of the various parameters used in the model. Due to the nature of the spontaneous formation of the quantum dots studied in this work, the ground state density denoted by $\rho(E)$ is given by a typical Gaussian distribution.

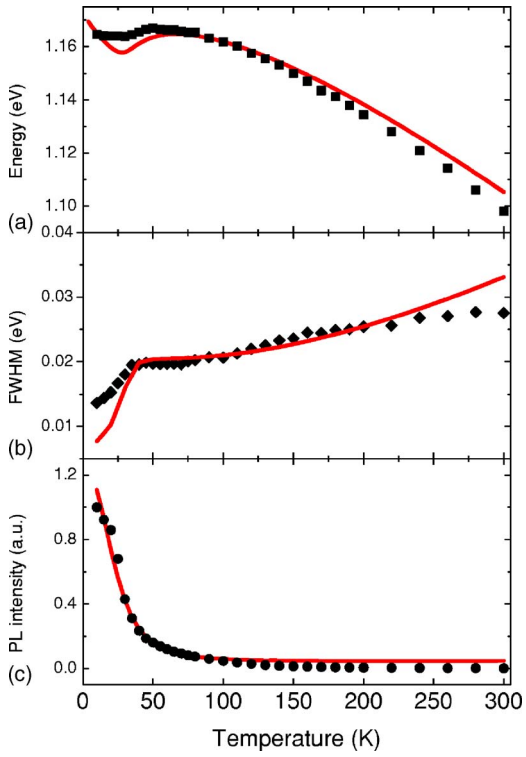

FIG. 5. (Color online) Temperature dependence of the PL spectral parameters of sample B: (a) energetic position, (b) FWHM, and (c) integrated intensity. The solid symbols are the experimental data, while the solid lines represent the calculated results using the localized-state luminescence model.

Such a distribution is characterized by a central energy E_0 and a linewidth relevant parameter σ. Under steady state condition and taking into account the radiative recombination (rate $1/\tau_r$), thermal escape (rate $1/\tau_{\mathrm{tr}} \exp[(E-E_a)/k_BT]$), and recapture of the localized carriers, the distribution function of the localized carriers can be derived as $f(E,T)=1/\{\exp[(E-E_a)/k_BT]+\tau_{\mathrm{tr}}/\tau_r\}$, where E_a is a special energy depending on the material and excitation level. The lineshape of the luminescence band is essentially given by $\rho(E)f(E,T)/\tau_r$. A more detailed description about the model can be found in Ref. 17. The core physical point of the model is that the thermal redistribution of carriers in localized states is responsible for the abnormal temperature behavior of the emission band.[17,21]

It is now convenient to discuss the temperature dependence of the three key spectral parameters, namely, peak position, linewidth, and integrated intensity, of the luminescence band. It is well known that the temperature dependence of the fundamental band gap of a perfect semiconductor can be predicted by Varshni empirical formula $E_g=E_0-\alpha T^2/(\Theta+T)$, where α and Θ are the so-called Varshni parameter and Debye temperature of the material, respectively. The Varshni formula predicts a monotonous shrinking of the fundamental band gap of the material with temperature, in contrast to the experimental data shown in Figs. 4 and 5. For the luminescence peak position of materials with localized states, a correction caused by the thermal redistribution of the localized carriers must be added to the prediction of the Varshni formula. After taking the correction into consideration, the luminescence peak position of localized carriers can be described by $E_{\mathrm{PL}}=E_0-\alpha T^2/(\Theta+T)-x(T)k_BT$. Here $x(T)$ is a dimensionless parameter whose value can be obtained by numerically solving the following nonlinear equation:[17,21]

$$xe^x=\left[\left(\frac{\sigma}{k_BT}\right)^2-x\right]\left(\frac{\tau_r}{\tau_{\mathrm{tr}}}\right)e^{(E_0-E_a)/k_BT}. \tag{1}$$

For the linewidth of the luminescence band, besides the inhomogeneous distribution of localized states, the broadening due to the impurity scattering as well as the acoustic-phonon and longitudinal-optical-phonon scatterings must be accounted for. Therefore, the linewidth of localized-state luminescence band can be determined by calculating the convolution of the lineshape function, $\rho(E)f(E,T)/\tau_r$, resulting from the inhomogeneous distribution of localized carriers and the broadening function due to phonon and impurity scattering.[17] The broadening function due to the impurity and phonon scattering is given by $[4E^2+\Gamma^2]^{-1}$, where $\Gamma=\Gamma_0+\eta_AT+\eta_{\mathrm{LO}}/[\exp(\hbar\omega_{\mathrm{LO}}/k_BT)-1]$. Here Γ_0 is a constant that accounts for the impurity or imperfection scattering; η_A and η_{LO} are the acoustic-phonon and longitudinal-optical-phonon scattering coefficients, respectively; and $\hbar\omega_{\mathrm{LO}}$ is the characteristic energy of the longitudinal optical phonon.[24]

Finally, the normalized integrated intensity of the localized-state luminescence band is given by[17]

$$I_{\mathrm{PL}}=\frac{1}{1+(1-\gamma_c)\exp\{[(E_0-E_a)+k_BT\ln(\tau_r/\tau_{\mathrm{tr}})]/\sqrt{(k_BT)^2+2(\sigma/2.41)^2}\}}, \tag{2}$$

where γ_c is the recapture coefficient of the already escaped carriers by the localized states.

For sample A, we adopted values of the parameters as follows: $E_0=1.13$ eV, $E_a-E_0=0.075$ eV, $\sigma=0.021$ eV, $\tau_{\mathrm{tr}}/\tau_r=0.027$ ps/300 ps, $\alpha=0.48$ meV/K, and $\Theta=270$ K to calculate the temperature dependence of the luminescence peak position using the model described above. For the linewidth calculation, $\Gamma_0=0.01$ eV, $\eta_A=0.0012$ meV/K, $\eta_{\mathrm{LO}}=0.4$ eV, and $\hbar\omega_{\mathrm{LO}}=36$ meV were taken, and for the integrated intensity fitting, the value of $\gamma_c=0.1$ was adopted. The calculated results are depicted as solid lines in Fig. 4, where good agreement between the experimental and theo-

retical results can be seen. For sample B, the values of the various parameters adopted in modeling the experimental results are shown below. For the peak position calculation, $E_0=1.182$ eV, $E_a-E_0=-0.009$ eV, $\sigma=0.008$ eV, $\tau_{tr}/\tau_r=0.142$ ps/300 ps, $\alpha=0.47$ meV/K, $\Theta=270$ K; for the linewidth calculation, $\Gamma_0=0.003$ eV, $\eta_A=0.0012$ meV/K, $\eta_{LO}=0.057$ eV, and $\hbar\omega_{LO}=36$ meV; for the integrated intensity fitting, $\gamma_c=0.989$. The calculated curves are shown in Fig. 5 by the solid lines. Again, a good agreement between theory and experiment is achieved for sample B. As expected, the key parameters of samples A and B show some significant differences. Comparison and discussion of these key parameter values, such as E_a, are important to obtain a deeper understanding of the luminescence mechanisms for the two kinds of GaInAsN QDs.

As mentioned earlier, the localized-state luminescence model was developed based on a distribution function.[17] Among all the parameters used in the model, E_a, the critical energetic level below which all the localized states are occupied at 0 K is of great importance. The distribution function of localized carriers possesses a similar expression to the Fermi-Dirac distribution function. To some extent, E_a in this function is just like the Fermi level in the Fermi-Dirac distribution function. The position of E_a relative to the central energy (E_0) of the density of states for the localized carriers has a decisive influence on the temperature dependence of the PL peak position. As for sample A, the value of $E_a-E_0=0.075$ eV was adopted, that is, E_a is 75 meV higher than E_0. This value is close to the thermal activation energy of 72 meV obtained by Yew *et al.* from the temperature-dependent integrated PL intensity curve of the GaInAsN QDs using a well-known model for describing the thermal quenching of luminescence for a two-level system.[13] In fact, it has been proven that Eq. (2) reduces to the two-level luminescence thermal quenching formula when the parameter σ approaches zero.[17] It has been argued that the wetting layer in self-assembled QDs predominately determines the energy level E_a. In sharp contrast to sample A, a value of $E_a-E_0=-9$ meV was taken for sample B. In other words, E_a is located at 9 meV below the central energy position of the localized-state distribution. From the physical viewpoint, it is entirely possible for the cases with $E_a-E_0<0$ to exist in real material systems. As discussed in the literature, when E_a is less than E_0 a typical "S-shaped" temperature dependence of the luminescence peak position appears.[17,22,23] At the same time, a strong asymmetric lineshape of the luminescence band at low temperatures is observed as seen in Fig. 3. Based on the above, one obtains a physical picture of the electronic structures and optical transitions for both samples at 0 K, as shown in Fig. 6. For sample B with $E_a<E_0$, the carriers can thermally excite to the higher localized states above E_a as the temperature increases. As a consequence, the luminescence band would broaden rapidly. When the temperature is above 40 K, the phonon-assisted escape of carriers out of the localized states becomes noticeable and results in a narrowing of the PL band. This narrowing can be largely compensated by the broadening due to the phonon scattering, such that the PL linewidth remains unchanged and a plateau region appears in the temperature dependence curve. As the temperature is further increased, the effect of longitudinal-optical-phonon scattering on the broadening of the PL band becomes dominant. Consequently, the linewidth of the PL band increases again.

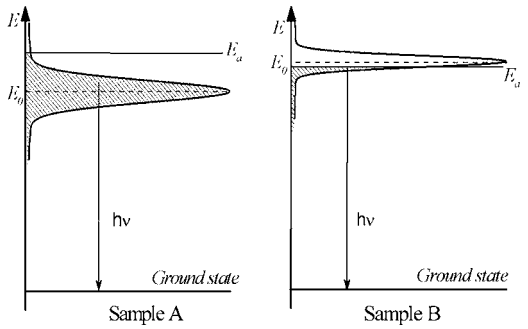

FIG. 6. Schematic diagrams of electronic structures and optical transitions for samples A and B at 0 K.

Now we turn to discuss the temperature dependence of the PL intensity. As shown in Fig. 3, the emission signal of sample B can be clearly observed at temperatures up to 300 K, while the PL signal of sample A becomes unobservable for temperatures beyond 220 K. Clearly, the luminescence band of sample A thermally quenches faster. An explanation for this phenomenon can be obtained from the values of relevant parameters used in the modeling. In the model the ratio of τ_{tr}/τ_r is a key parameter that determines the thermal quenching rate of the luminescence band. τ_{tr} and τ_r characterize the thermal escape of carriers from the localized states and the radiative recombination of the localized carriers, respectively. It should be noted that in the calculations the same $\tau_r=300$ ps was adopted for the two samples, while the value of τ_{tr} for sample A is taken as 0.027 ps and that for sample B as $\tau_{tr}=0.142$ ps. Clearly, the relevant rate $1/\tau_{tr}$ which stands for the possibility of the localized carriers attempting to escape thermally from localized states is much higher for sample A. This means that the luminescence of sample A has a faster thermal quenching rate. Indeed, the experimental observation is in agreement with this theoretical expectation. Another important parameter is the recapture coefficient γ_c of already escaped carriers by the localized states. The fitted γ_c value ($\gamma_c=0.1$) for sample A is much less than that ($\gamma_c=0.989$) for sample B. The lower recapture coefficient also leads to the faster thermal quenching of the luminescence band. Therefore, both the higher thermal escape rate of the localized carriers and the lower recapture rate of the already escaped carriers are responsible for the observed faster quenching of the luminescence band of sample A.

Since the distribution profile of localized carriers essentially determines the lineshape of the luminescence band according to the model, a direct comparison of the spectral shapes between the experimental luminescence spectra and calculated distribution of localized carriers is interesting. Figure 7(a) shows the calculated distribution profiles of localized carriers at several typical temperatures for sample B, while the measured PL spectra of sample B are plotted in Fig. 7(b). Note that the intensities of the distribution profiles and PL spectra are normalized, and the peak positions are manually coincided so that the lineshape evolution with tem-

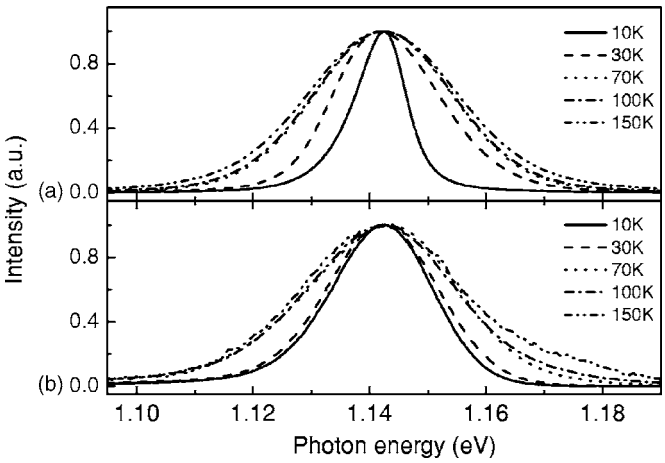

FIG. 7. (a) Calculated distribution profiles of the localized carriers at different temperatures. (b) Measured PL spectra of sample B at same temperatures. The peak positions of calculated profiles and experimental spectra are manually coincided for clarity.

perature can be clearly seen. From Fig. 7(a), it can be seen that the thermal redistribution of localized carriers leads to an asymmetric broadening of the distribution profiles as the temperature is elevated. At low temperatures, the distribution profile of the localized carriers exhibits a typical asymmetric lineshape with a sharp higher energy edge and a lower energy tail. When the temperature is increased the higher energy edge of the distribution profile broadens more rapidly than the lower energy edge. As a result, the distribution of the localized carriers tends to become symmetric and then retains this symmetry in the moderately high temperature range. As shown in Fig. 7(b), the variable-temperature PL spectra of sample B basically reflect such an evolution of the carriers' distribution profile.

IV. SUMMARY

The optical properties of two kinds of GaInAsN QDs with different compositions and growth thicknesses have been studied through their variable-temperature PL spectra. It has been found that the temperature dependence of the luminescence bands of the two samples is quite different. Using a localized-state luminescence model, we have quantitatively interpreted the observed temperature-dependent spectral features including the peak position, linewidth, and integrated intensity. This interpretation has revealed that it is the difference in the electronic structure of the two QD samples that leads to the significantly different temperature dependence of their luminescence bands. These results show that the localized-state luminescence model is very useful for understanding the complicated spontaneous emission mechanisms in real material systems.

ACKNOWLEDGMENTS

This work was financially supported by HK-RGC CERG Grants under Contract No. HKU 7049/04P. One of the authors (S.J.X.) wishes to acknowledge Professor W. J. Fan for providing the samples investigated in the present study. He is also grateful to Professor C. D. Beling for his critical reading and correcting the English of this paper.

[1]M. Kondow, K. Uomi, A. Niwa, T. Kitatani, S. Watahiki, and Y. Yazawa, Jpn. J. Appl. Phys., Part 1 **35**, 1273 (1996); M. Kondow, T. Kitatani, S. Nakatsuka, M. C. Larson, K. Nakahara, Y. Yazawa, M. Okai, and K. Uomi, IEEE J. Sel. Top. Quantum Electron. **3**, 719 (1997).
[2]See, for example, a recent review article, J. S. Harris, Jr., Semicond. Sci. Technol. **17**, 880 (2002).
[3]M. Kondow, S. Natatsuka, T. Kitatani, Y. Yazawa, and M. Okai, Electron. Lett. **32**, 2244 (1996).
[4]S. Sato, Y. Osawa, T. Saitoh, and I. Fujimura, Electron. Lett. **33**, 1386 (1997).
[5]M. C. Larson, M. Kondow, T. Kitatni, N. Nakahara, K. Tamura, H. Inoue, and K. Uomi, IEEE Photon. Technol. Lett. **10**, 188 (1998).
[6]H. P. Xin, K. L. Kavanagh, Z. Q. Zhu, and C. W. Tu, Appl. Phys. Lett. **74**, 2337 (1999).
[7]X. Yang, M. J. Jurkovic, J. B. Heroux, and W. I. Wang, Appl. Phys. Lett. **75**, 178 (1999).
[8]G. L. Belenky *et al.*, IEEE J. Quantum Electron. **35**, 1515 (1999).
[9]M. Sopanen, H. P. Xin, and C. W. Tu, Appl. Phys. Lett. **76**, 994 (2000).
[10]T. Hakkarainen, J. Toivonen, M. Sopanen, and H. Lipsanen, Appl. Phys. Lett. **79**, 3932 (2001).
[11]M. Fischer, M. Reinhardt, and A. Forchel, IEEE J. Sel. Top. Quantum Electron. **7**, 149 (2001); M. Fischer, M. Reinhardt, and A. Forchel, Electron. Lett. **36**, 1208 (2002); D. Gollub, M. Fischer, and A. Forchel, Electron. Lett. **38**, 1183 (2002).
[12]Y. Ikenage, T. Miyamoto, D. Nakino, T. Kayeyama, M. Arai, F. Koyama, and K. Iga, Jpn. J. Appl. Phys., Part 1 **41**, 664 (2002).
[13]K. C. Yew, S. F. Yoon, Z. Z. Sun, and S. Z. Wang, J. Cryst. Growth **247**, 279 (2003).
[14]Z. Z. Sun, S. F. Yoon, K. C. Yew, B. X. Bo, A. Y. Du, and C.-H. Tung, Appl. Phys. Lett. **85**, 1469 (2004).
[15]G. Bais, A. Cristofoli, F. Jabeen, M. Piccin, E. Carlino, S. Rubini, F. Martelli, and A. Franciosi, Appl. Phys. Lett. **86**, 233107 (2005).
[16]Z. F. Wei, Q. Li, S. J. Xu, S. F. Yoon, and W. J. Fan (unpublished).
[17]Q. Li, S. J. Xu, M. H. Xie, and S. Y. Tong, Europhys. Lett. **71**, 994 (2005).
[18]K. Kim and A. Zunger, Phys. Rev. Lett. **86**, 2609 (2001).
[19]P. R. C. Kent and A. Zunger, Phys. Rev. Lett. **86**, 2613 (2001).
[20]Z. F. Wei, S. J. Xu, R. F. Duan, Q. Li, J. Wang, Y. P. Zeng, and H. C. Liu, J. Appl. Phys. **98**, 084305 (2005).
[21]Q. Li, S. J. Xu, W. C. Cheng, M. H. Xie, S. Y. Tong, C. M. Che, and H. Yang, Appl. Phys. Lett. **79**, 1810 (2001).
[22]S. J. Xu, Q. Li, J.-R. Dong, and S. J. Chua, Appl. Phys. Lett. **84**, 2280 (2004).
[23]Q. Li, S. J. Xu, M. H. Xie, and S. Y. Tong, J. Phys.: Condens. Matter **17**, 4853 (2005).
[24]S. Rudin, T. L. Reinecke, and S. Segall, Phys. Rev. B **42**, 11218 (1990).